Electrochemical behavior of CoS and RGO anchored CoS nanoflowers synthesized via hydrothermal method

D. Govindarajaran[1*] and Joseph Selthraj[1]
[1]Department of Physics, Annamalai University, Annamalai Nagar-608002, Tamil Nadu, India.
Corresponding email*:degerajan@gmail.com

Abstract

In situ synthesis of pure CoS@180°C and RGO/CoS@180°Cnanocomposite was synthesized through hydrothermal method. The synthesized nanocomposite were characterized by spectroscopic (XRD, FTIR, RAMAN, SEM and HRTEM) and electrochemical techniques. The XRDspectra confirm the hexagonal structure of CoS@180°C and RGO/CoS@180°Cnanocomposite. All the diffraction peaks are very well coincid with JCPDScard No. 75-0605. FTIR spectrum shows the characteristic peaks are spotted at 422, 553 and 1092 cm^{-1} for RGO/CoS@180°C. The Raman spectrum also confirms the formation of CoS@180°C and RGO/CoS@180°Cnanocomposite. The flower like shapes was seen through SEM and HRTEM images. The higher specific capacitance values of RGO/CoS@180°C electrode than CoS electrode is due to RGO nanosheets support the huge surface area with good mesoporosity, which increasesthe electron and ion mobility during the redox process.

Keywords: hexagonal; XPS; EDAX; SEM; HRTEM;Specific capacitance.
DOI Number: 10.48047/NQ.2022.20.17.NQ880170 **Neuroquantology 2022; 20(17):1350-1366**

1. Introduction

Presently, demands for energy storage devices are being increased and the scientific community has more focused on super capacitors (SCs). Compared to conventional batteries, SCs have lot advantages such as huge power and energy density, easy operation, high cycle stability with eco-friendly nature[1-2]. The efficiency of both batteries and capacitors are compensated by the performance of SCs alone [3]. For the miniaturized electronics, batteries and capacitors are not housed due to their weight and thickness [4]. So that, scientist are more preferably used SCsas apotential candidate to all electronic equipments [1-4].SCs are mainly categorized in two based on its charge storage process. One is pseudocapacitor (Faradic processes) and another one is Eclectic double layer (EDLC) (Non- Faradic processes). Compared with EDLC, pseudocapacitor delivered high specific capacitance, high power and energy density due to its faradic reaction [5-7].

Previously, different phases of cobalt sulfide (CoS, CoS_2, Co_3S_4, Co_8S_9) have been explored widely for energy conversion. Especially, CoS can be used for SCs due to its outstanding redox capability and less cost effect [8-10]. Some of the drawbacks arise while it undergoes the electro chemical process, like

pulverization, less electrical conductivity, rapid capacity decay and inadequate specific capacitance [11-13]. To overcome these problems, numerous researchers have concentrated on the desirable design of CoS nanomaterial with noval structure and active composites [14-16]. In particular, carbon based materials has employed as an active material for the improved capacitive performance [17-19]

Graphene/graphene oxide (GO) is a 2D single nanosheet like structure and it has unique property such as highmechanical flexibility and good conductivity and mainly used as an active material for SCs electrode. At present, reduced graphene oxide (RGO) is extensively used as an active material for the preparation of nanocompositeand also it has good electrochemical properties. Previously, lot of researchers are prepared the RGO/CoS nanocomposite and utilized in the field of SCs. For instance, Qu B et al., prepared graphene oxide decorated β-CoS via hydrothermal process along with Ar calcinations method for SCs application [20]. Shi J et al., synthesized CoS/GO composite network and coated on nickel foam by electrochemical deposition and its exhibit high specific capacitance and outstanding rate capability [21]. Hybrid RGO/CoS composite delivers high specific capacitance value of 550 F/g at 1 A/g current density [22]. 3D based RGO/CoS_x nanoflakes exhibit less crystallinity with specific capacitance of 443 F/g at 1 A/g [23]. Although, a lot of efforts has been taken to overcome the high preparative cost, low crystallinity, inadequate specific capacitance and the reduce length of the experimental process.

In the present study,a simple hydrothermal method is used to prepare aCoS nanoparticles (NPs)at different temperatures (140, 160 and 180°C) and the sample synthesized at 180°C is utilized to make RGO/CoS nanocomposite and characterized by different techniques.

2. Materials and Methods

For the preparation of Cobalt sulfide nanoparticles, the precursors of Cobalt nitrate hexahydrate and thiourea were purchased from Sigma Aldrich Company. Graphite powder, potassium permanganate, sodium nitrate, hydrogen peroxide (H_2O_2), sulfuric acid, hydrochloric acid, hydrazine hydrate (N_2H_4), polyvinylidenedifluoride (PVDF), *N*-methyl-2-pyrrolidone (NMP) and acetylene black were purchased from Merck India Pvt. Ltd. All the chemicals are analytical grade of 99.9% purity.

2.1. CoS preparation

2.91 g of Cobalt nitrate and 0.76 g of thiourea were dissolved in 50 ml of DI water. The above mixed solution was stirred until it reached homogenously. The obtained homogenous solution was transferred into 100 ml teflon coated autoclave and heated at 140°C for 24 hrs. Finally, the residue (CoS) was collected and washed many times with DI water and ethanol and dried in an oven at 80°C for 5hrs. The obtained product is designated as CoS@140°C. The same procedure is repeated for the preparation CoS heated at 160°C and 180°C and the obtained product are named as CoS@160°C and CoS@180°C.

2.2. RGO preparation

The GO preparation was done by the modified Hummer's method [24]. The pure graphite powder and sodium nitrate were dissolved in 50 ml of sulfuric acid and stirred it for 5hrs in the ice bath setup. After 30 minutes,6g of potassium permanganate were added gradually. After 5 hrs the beaker was taken out from the ice bath and stirred at 80°C. Once it reaches the prescribed temperature, 100 ml of DI water was slowly added and stirred it continuously for 3hrs. Finally, 50 ml of hydrogen peroxide was added and the solution turns become brilliant yellow colour. Finally, the

obtained GO flushed with deionised water and heated in oven at 80°C for 5hrs. The Prepared GO was reduced by adding the reducing agent hydrazine hydrate and transferred to ultrasonification. Then the Reduced GO was used for the further characterization.

2.3. RGO/CoS preparation

The prepared CoS@180°CNPs and RGO samples were dissolved in 50 ml of DI water and stirred it for 3hrs and maintained the temperature at 80°C. Then the dried compositeflushed withdeionized waterfor several times. The final product is designated as RGO/CoS@180°C.

2.4. Electrode preparation

For the electrode preparation, the CoS@180°CNPs, PVDF and acetylene black was taken with the ratio of 80:10:10 respectively and grinded it evenly. The few drops of NMP solution were added and again it grind well until it reach in slurry form. Once it reaches, the slurry was coated on nickel plate (1 cm X 1 cm) and dried at 90°C for 10hrs. Then the coated plate was used as the working electrode for the electrochemical measurement. The same procedure is repeated for preparing RGO/CoS@180°C nanocomposite electrode.

3. Results and Discussions

3.1. Structural analysis

Fig. 1 represents the XRD spectrum of as prepared CoS at three different temperatures 140°C, 160°C and 180°C.The XRD peaks are observed at 30°, 34°, 35°,46° and 54°are related to the planes at (100), (002), (101), (102) and (110), respectively. The observed planes clearly evident that the synthesized CoSisformed with hexagonal crystal structureaccording to JCPDS Card No. 75-0605 [27 - 31]. Also, the XRD peaks indicate that the CoS sample synthesized at 140°Care not well formed. As temperature increases to 180°C the XRD peaks appeared as sharp indicating that the prepared CoS@180°Care highly crystalline and pure without any impurities compared to CoS@140°C and CoS@160°C. The d spacing value of the intense XRD peak appeared at 2θ = 46° is 0.49 nm.

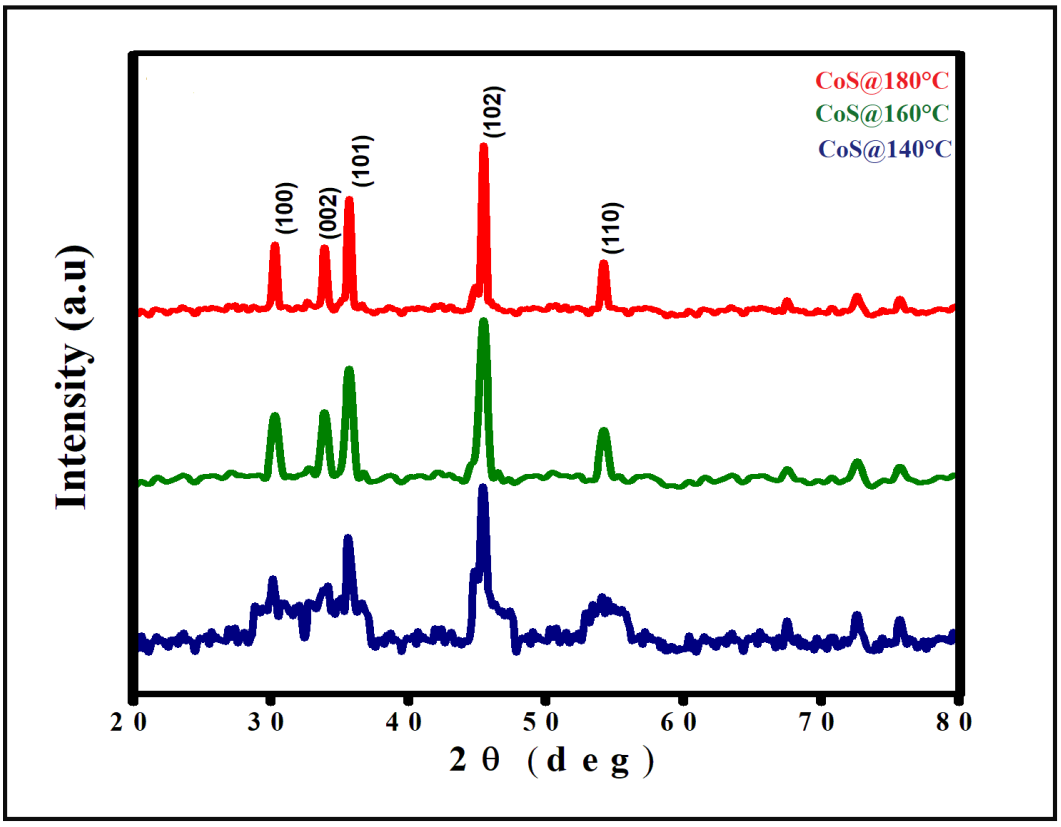

Fig. 1: XRD spectrum of CoS synthesized at three different temperatures 140ºC, 160ºC and 180ºC.

The structural parameters of CoS NPs are evaluated using the following equations [32 - 36].

Crystallite Size $D = \frac{K\lambda}{\beta \cos\theta} = \frac{0.9\lambda}{\beta \cos\theta}$ … (1)

Where 'λ' is the Wavelength, '*β*' is the Full width half maximum, and 'θ' is the Bragg's angle.

Microstrain $\varepsilon = \frac{\beta cos\theta}{4}$ … (2)

Dislocation density $\delta = \frac{1}{D^2}$ … (3)

Where n is equal to unity and D is the crystalline size.

Lattice parameters $\frac{1}{d_{hkl}^2} = \frac{h^2}{a^2} + \frac{k^2}{b^2} + \frac{l^2}{c^2}$ … (4)

Where, 'd_{hkl}'represents the interplanar spacing and '*hkl*'is the Miller indices.

The calculated structural parameters of the synthesized CoS at 140°C, 160°C and 180°Care listed in **table.1**.

Table 1: Structural parameters of CoS

SampleNotations	Crystalline size D (nm)	Microstrain × 10^{-3}	Dislocation density × 10^{15} (lines/m^2)	Lattice parameters	
				a = b	c
CoS@140°C	22	1.9	2.1	3.66	5.27

CoS@160°C	26	1.6	1.9	3.43	5.20
CoS@180°C	28	1.4	1.8	3.36	5.14

From the **table 1**,it is noted that the reaction temperature increaseswith crystallite size, whereas the microstrain and dislocation density are decreases which indicates lesser imperfection in crystal lattice. From the evidential structural parameters, the prepared CoS@180°C nanoparticleis chosen for the preparation RGO/CoS@180°C nanocomposite.

Fig. 2 represents the XRD spectrum of CoS@180°Cand RGO/CoS@180°C nanocomposite. From the Fig. 2, it can be seen that one additional peak at 24° corresponding to (002) planes belonging to RGO, which clearly indicates in situ embedding ofCoS@180°C nanoparticles into RGO sheets occurs simultaneously, leading to the formation of a RGO/CoS@180°C nanocomposite. As observed from the **table 2**, the crystallite size of RGO/CoS@180°C nanocompositedecreases to 25 nm whereas microstrain and dislocation density increases from 1.4 x 10^{-3} to 1.5 x 10^{-3} and 1.8 x 10^{-3} to 2.0 x 10^{-3}lines/m^3 which is due to the inverse relation with crystalline size of nanocomposite. The other structural parameters almost remain constant for both CoS@180°C and RGO/CoS@180°C nanocomposite.

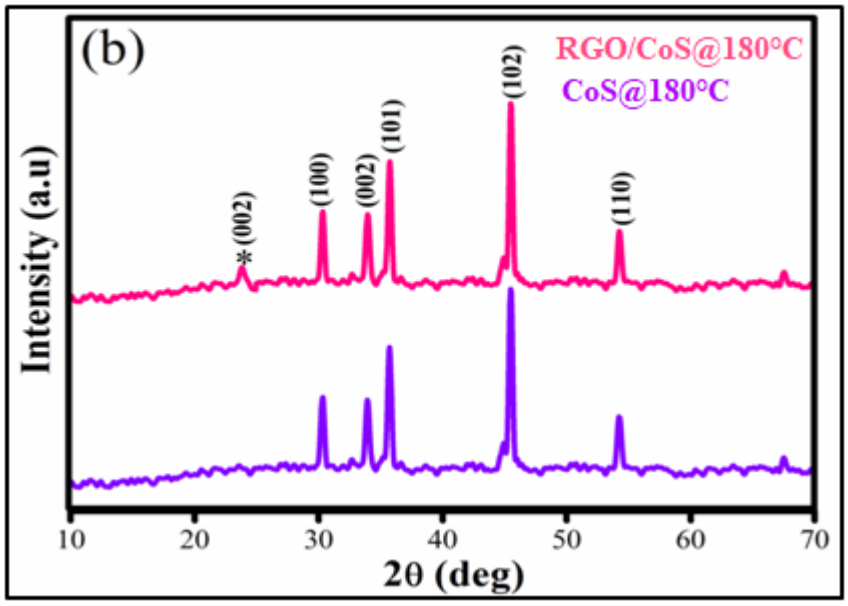

Fig. 2: XRD spectrum of CoS@180°Cand RGO/CoS@180°Cnanocomposite.

Further, the crystalline size and strain are calculated by Williamson-Hall (W-H) method using following equation [37, 38].

$\beta_{hkl}Cos\theta = \frac{K\lambda}{D} + 4\varepsilon.Sin\theta$ … (5)

Table 2: Structural parameters ofCoS@180°Cand RGO/CoS@180°Cnanocomposite.

Sample Notations	Crystalline size D (nm)	Microstrain × 10^{-3}	Dislocation density × 10^{15}	W-H Plot		Lattice parameters	Volume	Density
				D	ε ×			

			(lines/m^2)	(nm)	10^{-3}	a = b	c	V= abc	g/cm^3
CoS@180°C	28	1.4	1.8	27	2.5	3.36	5.14	50.25	5.94
RGO/CoS@180°C	25	1.5	2.0	24	2.6	3.35	5.18	50.35	5.94

Equation (5) is an uniform deformation model (UDM) equation, which gives the crystalline size and strain of the crystals. **Fig.3 (a & b)**exhibit plot of equation (5) in which β_{hkl}.Cosθ (vs) 4Sinθ corresponding to each composition. The slope gives the value of the intrinsic strain, whereas the intercept affords the crystallite size for CoS@180°C and RGO/CoS@180°Cnanocomposite. The crystallite sizes are calculated using UDM model for CoS@180°C and RGO/CoS@180°C nanocomposite are 27 nm and 24 nm, whereas the strain values are 2.5 x 10^{-3} and 2.6 x 10^{-3}, respectively. The values of crystalline size and strain calculated using W-H plot are consisted with values calculated using Debye Scherrer.

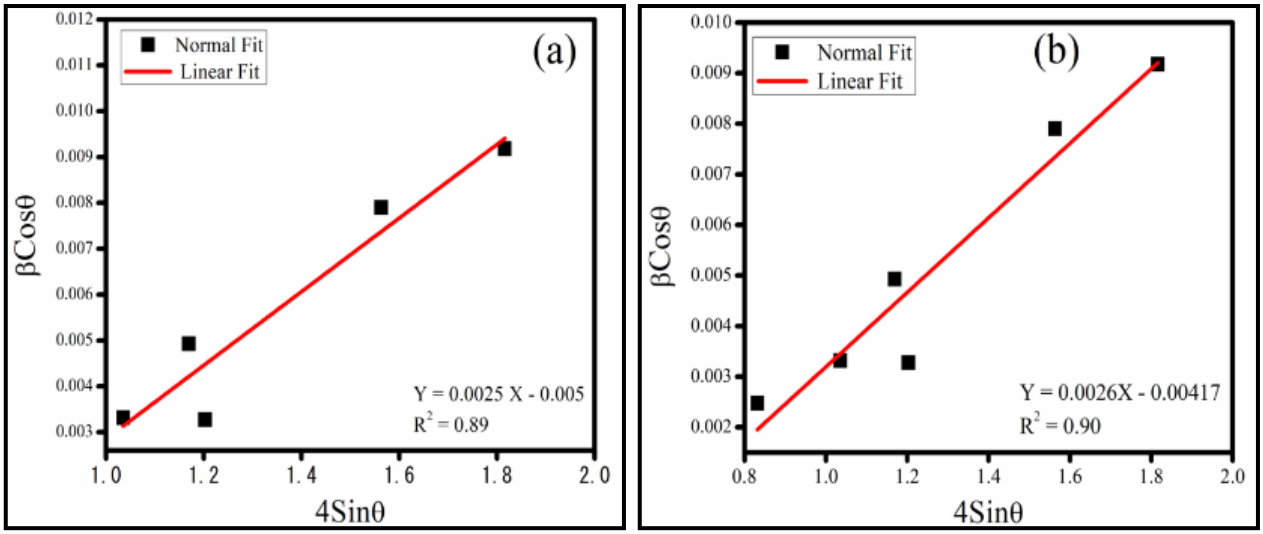

Fig. 3:W-H plot of a) CoS@180°Cand b) RGO/CoS@180°Cnanocomposite.

3.2. FTIR and Raman Spectroscopy

FTIR measurement was performed to study the vibrational properties and functional group analysis of CoS@180°Cand RGO/CoS@180°Cnanocomposite. From the **Fig. 4**, the IR bandsnoted in the CoS@180°C spectra are 422 cm^{-1}, 726 cm^{-1}, 843 cm^{-1}, 1155 cm^{-1}, 1504 cm^{-1}, 1632 cm^{-1} and 3389 cm^{-1} . The bands observed at 3389 cm^{-1} and 1632 cm^{-1} corresponds to the O-H stretching and bending vibrational modes of water molecules [39]. The band observed at 1155 cm^{-1} is related to symmetric and asymmetric of C-C and C-O-C vibrations in theCoS nanoparticles[40]. The band observed at 1504 cm^{-1} is assignment to a hydroxyl bending of different types of surface hydroxyl groups [41]. The peaks appeared at 422 cm^{-1} is related to CoS, 726 $cm^{-1}$and 843 cm^{-1} are related to N-C=S [42, 43]. Further, in the RGO/CoS@180°C nanocomposite (**Fig.4**), the characteristics peaks observed at553 $cm^{-1}$are related to CoS and 843 cm^{-1} are related to N-C=S. Also, the peak observed at 1092 cm^{-1} belongs to C-O which is strongly support the RGO formation inRGO/CoS@180°C Nanocomposite.

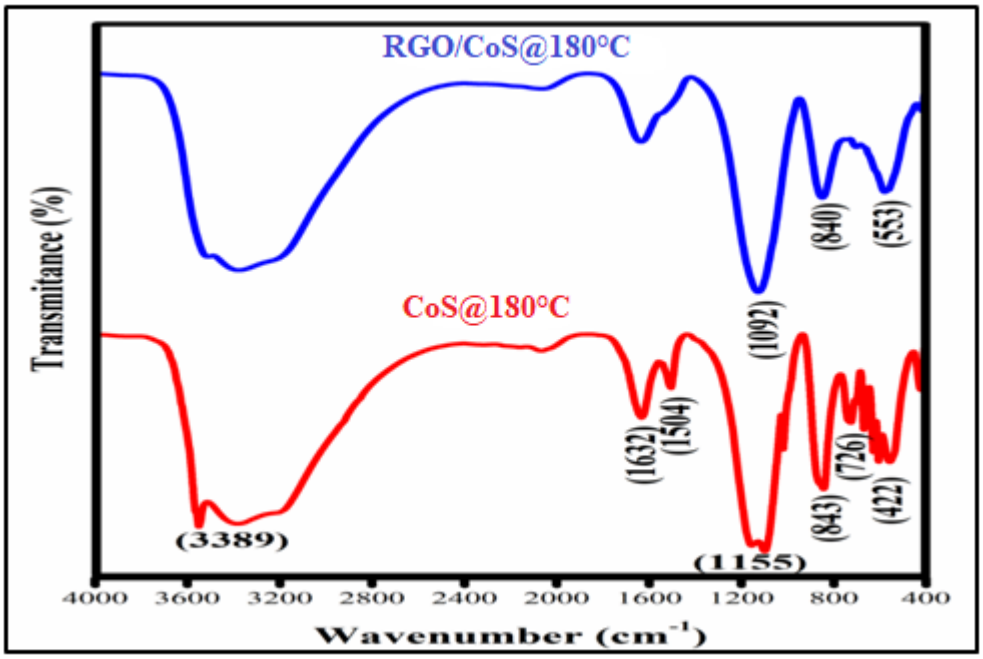

Fig.4: FTIR spectrum of CoS@180°C and RGO/CoS@180°C nanocomposite.

Fig. 5 shows the Raman spectra of CoS@180°C and RGO/CoS@180°C nanocomposite.Three Raman peaks are noted in the CoS@180°CNPsare 476 cm^{-1}, 516 cm^{-1} and 680 cm^{-1}. Among these, the small peaksappeared at 476 cm^{-1} and 516 $cm^{-1}$are consigned to $E_g$and F_{2g}modes and the third high intensity peak at 680 cm^{-1} is consigned to A_{ig} mode of CoS NPs [44]. Where as in the Raman spectra of RGO/CoS nanocomposite, two more additional peaks are appeared at 1337 cm^{-1} and 1598 cm^{-1} are assigned to D and G band of RGO. The G band is connected to bond stretching of sp2 carbon pairs in both rings and chains, while the D band is associated to the breathing mode of aromatic rings with dangling bonds in plane terminations, clearly indicates the successful formation of RGO/CoS@180°C nanocomposite[45 - 47].

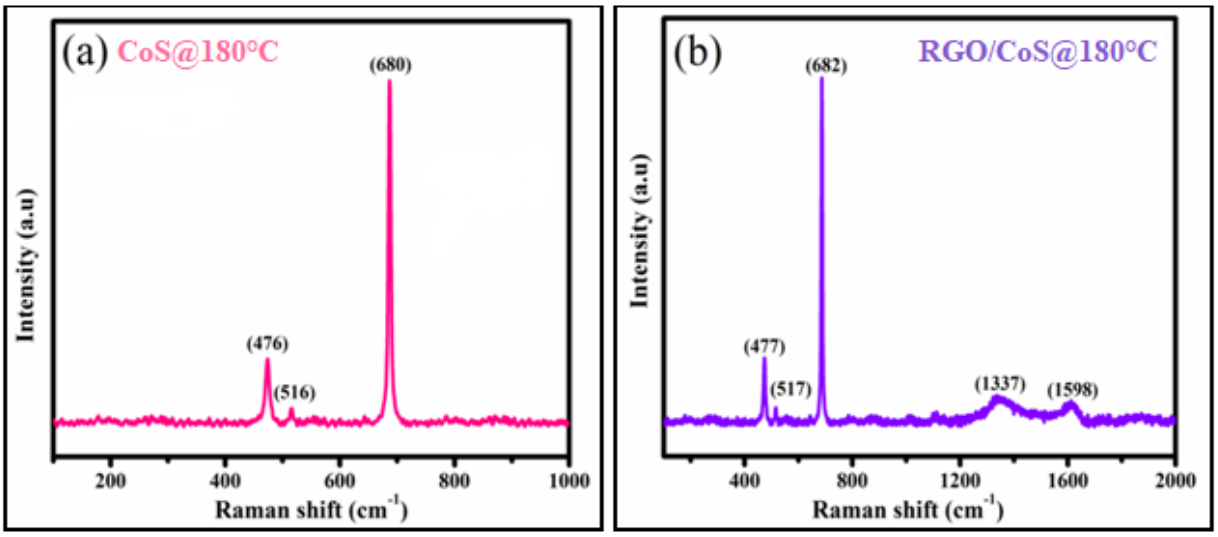

Fig.5: Raman spectra of a)CoS@180°C and b) RGO/CoS@180°C nanocomposite.

3.4. Morphological analysis

Fig. 6 (a - d) shows the SEM imagesCoS@180°C and RGO/CoS@180°C. **Fig.6 (a & b)**shows SEM imagesCoS@180°Cnanocomposite, which clearly indicate the formation of CoS nanoparticle like flower shapes. This may be due to assemblage of several nanosheets to form the flower-like structure. **Fig. 6(c&d)** shows SEM images of RGO/CoS@180°C nanocompositeare also appear like flower shape and are formed on the RGO nanosheets.The advantageous of sheet like flower is that it provides a large surface area for reactions and made it easier for target molecules to be transported and create active surface area for the capacitive performance [48].

Fig. 7(a - d) shows the TEM images of CoS@180°C and RGO/CoS@180°Cnanocomposite at different magnification also shows the flower like structure. These TEM images are evidently supporting the SEM images of CoS@180°Cand RGO/CoS@180°C nanocomposite. **Fig. 8(a - d)** shows the high resolution d spacing images and SAED pattern of CoS@180°C and RGO/CoS@180°Cnanocomposite in which d spacing values are 0.49 nm corresponding to the hkl plane (102) pattern. The results clearly matched with the XRD results.

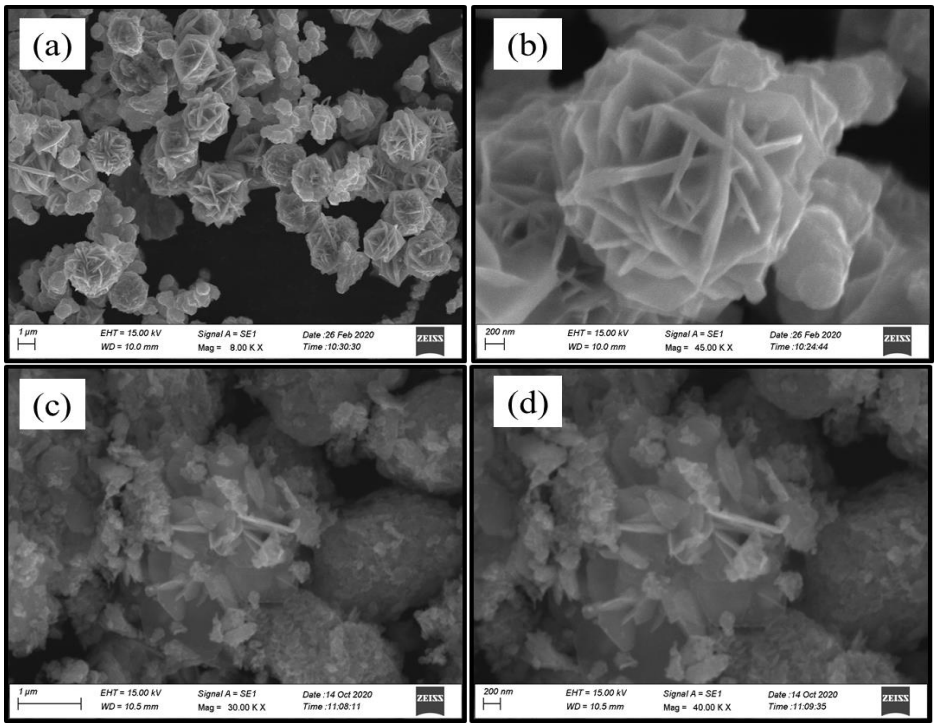

Fig. 6: (a & b) SEM images of CoS@180°C and (c & d) SEM images of RGO/CoS@180°C nanocomposite.

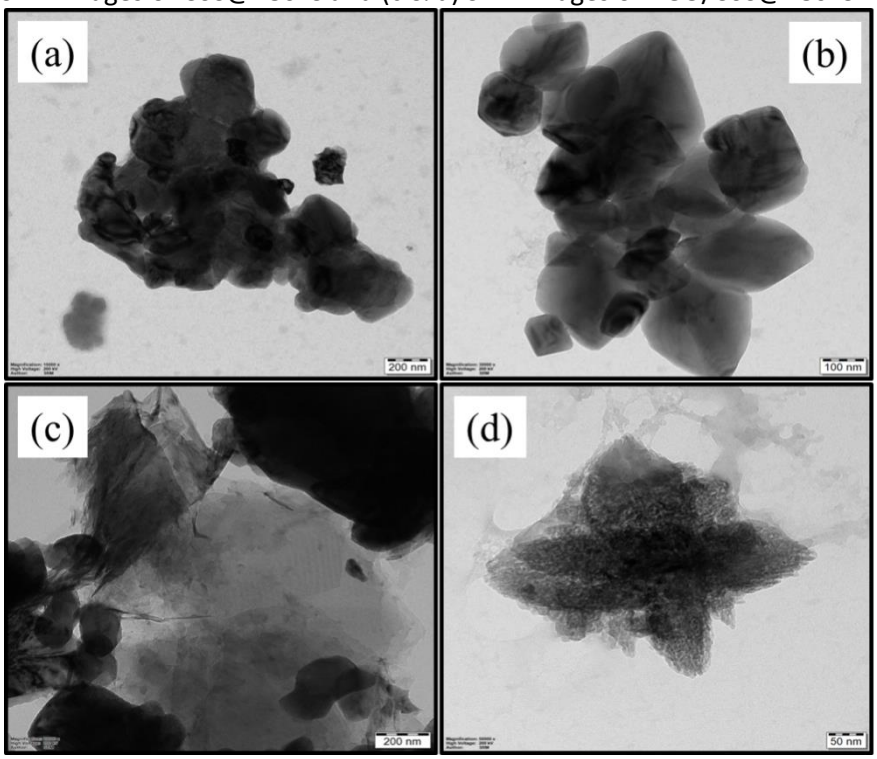

Fig. 7: (a & b) TEM images of CoS@180°C and (c & d) TEM images of RGO/CoS@180°C nanocomposite.

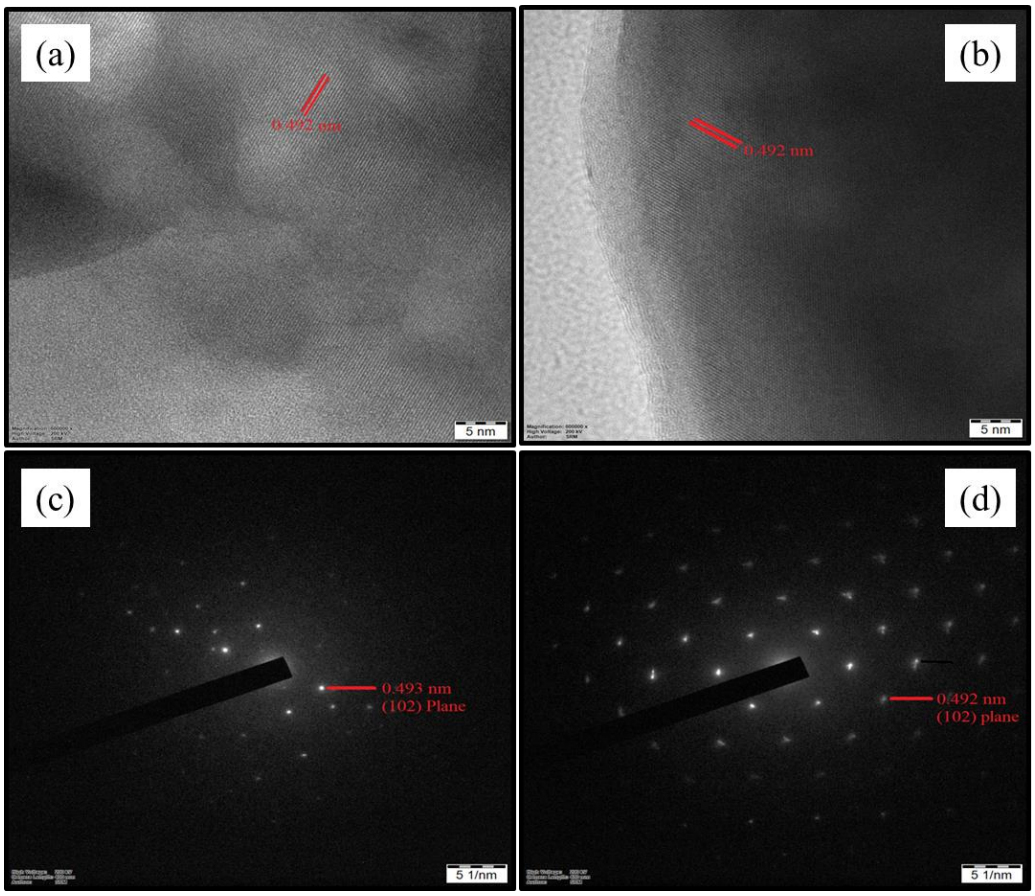

Fig. 8: (a – d) high resolution TEM images and SAED pattern of CoS@180°C and RGO/CoS@180°C nanocomposite.

3.6. Electrochemical performance

To explore the electrochemical properties of CoS@180°C and RGO/CoS@180°CNanocomposite, the fabricated electrodes were subjected into 6M KOH electrolyte solution and characterized by cyclic voltammograms (CVs) **Fig.9(a& b)** represents the CV curve ofCoS@180°C and RGO/CoS@180°C nanocompositeelectrodes. The CV curves of both of these electrodes shows oxidation and reduction peaks displays pseudocapacitive nature. The area under CV curve for the both electrodes increases and still remains similar shape demonstrating a favorable high-rate performance.It is observed that the position and shape of theredox peaks remain unchanged, indicating thatthere is continuous charging and discharging kinetics inthe redox reaction. If the scan rate is increased the peak current density is also increased. It is a result of the exchange of charge in a faradic reaction at theelectrode and electrolyte interface. The anode and cathode potentials were observed to be drifting in the positive direction due to the higher scan rate and the internal diffusion resistanceof cobalt-sulfide composite. The chemical reaction occurs during the process is likely due to the oxidations of CoS to CoSOH and CoSOH to CoSO, and two plausible reactions areproposed for electrochemical reactions [49, 50].

CoS (II) + OH^- ↔ CoSOH (III) + e^- … (6)

CoSOH (III) + OH^- ↔ CoSO (IV) +H_2O + e^- … (7)

The specific capacitance (C_p) of CoS@180°Cand RGO/CoS@180°C nanocompositeelectrodes can be calculated by using theequation [33]:

$$C_p = \frac{A}{m\Delta V} \quad \ldots (8)$$

Where C_p , A, m and ΔV represents cathodic and anodic charge on each scan rate, area under CV curve, mass of the active material (mg) and scan rate in mV/s. Using the above equation, the $C_p$values of CoS@180°Celectrode are calculated as 467 F/g, 398 F/g, 302 F/g, 229 F/g and 156 F/g, and the C_p values of RGO/CoS@180°C nanocomposite electrode are 650 F/g, 539 F/g, 452 F/g, 326 F/g and 230 F/g at a scan rates of 10, 30, 50, 75 and 100 mV/s, respectively. The calculated values of C_p show a decreasing trend from lower to higher scan rate which is mainly attributed due to the diffusion effect. **Fig. 9c** represents the $C_p$versus scan rate of CoS@180°C and RGO/CoS@180°C nanocompositeelectrodes and it can be clearly seen that the C_p of RGO/CoS@180°C nanocompositeelectrode is higher than that of CoS@180°Celectrode, which is due to the electron transfer efficiency and an increase in electrical conductivity [51].

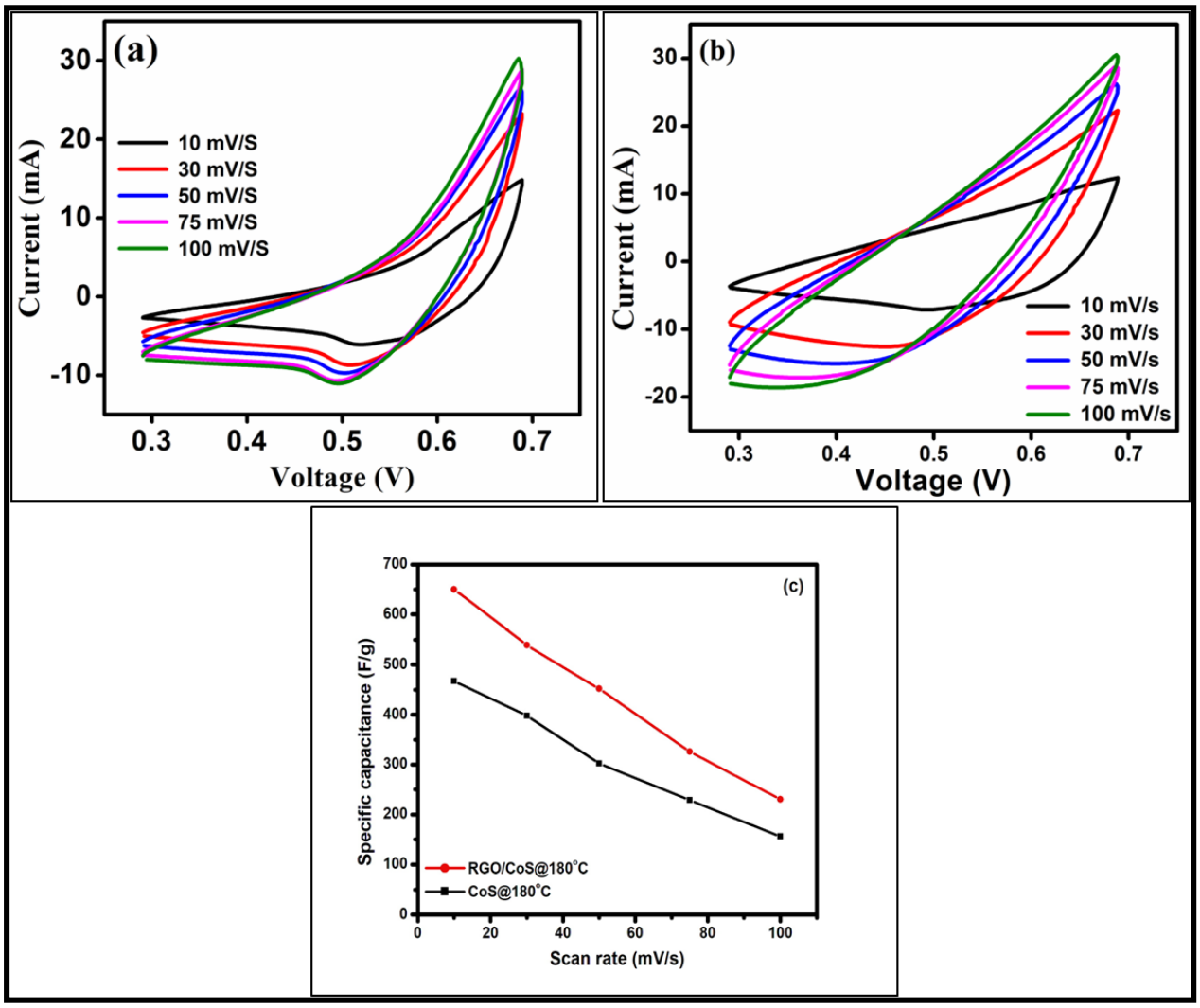

Fig. 9: (a & b) CV curves of CoS@180°C and RGO/CoS@180°C nanoconposite electrode.(c) Specific capacitance verses scan rate of CoS@180°Cand RGO/CoS@180°C nanocmposite electrodes.

Fig. 10 a and b represents the GCDs curves of CoS@180°C and RGO/CoS@180°C nanocompositeelectrodes at the current density of 2 A/g, 4 A/g, 6 A/g, 8 A/g and 10 A/g with the potential window varied from 0.3 V to 0.7 V. The $C_p$of CoS@180°C and RGO/CoS@180°C nanocompositeelectrodes using GCDs can be calculated from the following equation [32]:

$$C_{p\,(GCD)} = \frac{i\Delta t}{m\Delta V} \quad \ldots (9)$$

Where i is the current density (A/g), Δt is the discharging time (s), m is the mass of the active material (mg) and ΔV is the potential window (volts). The calculated C_p values of CoS@180°C and RGO/CoS@180°C nanocomposite electrode are 452F/g, 383 F/g, 295 F/g, 203 F/g, 136 F/g and 633 F/g, 496 F/g, 412 F/g, 305 F/g, 207 F/g, respectively. The $C_p$value decreases with increase of current density (**Fig. 10c**)which is partly due to the

increase in the incremental voltage drop and partly due to the deficiency of active sites related with redox reaction. Also the OH^- ion dispersion is high at lower current density and it takes adequate time to diffuse the whole energetic electrode which supports to increase of $C_p$value [52]. Moreover, the C_p of a RGO/CoS@180°C nanocompositeelectrode has a larger $C_p$value than CoS@180°C electrode, indicating that RGO boost the supercapacitive performance of the CoS@180°Celectrode. This may due to RGO sheets provide a large surface area with good mesoporosity that increases electron and ion mobility during the redox process [52].

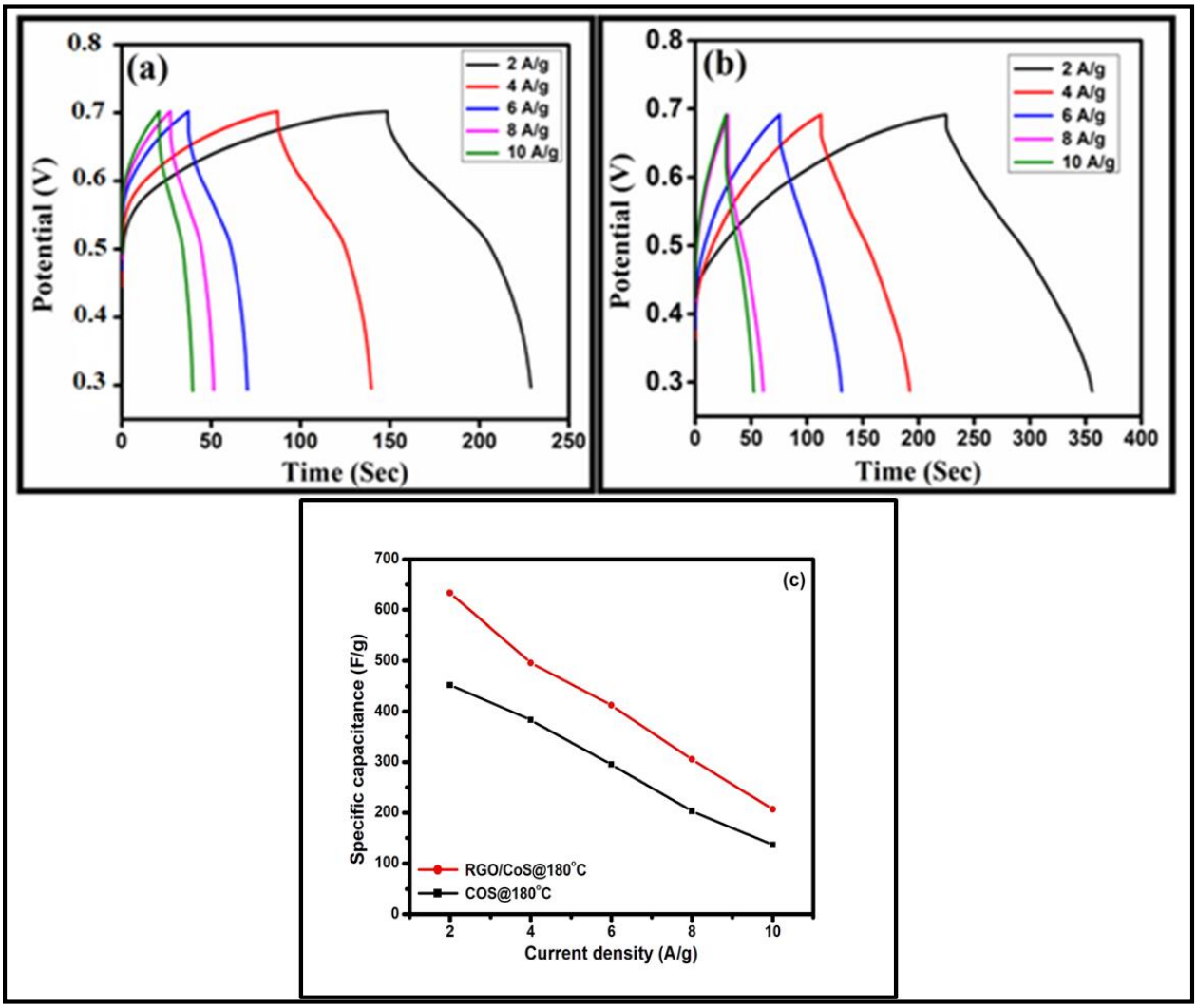

Fig. 10: (a & b) GCDs curves of CoS@180°C and RGO/CoS@180°C nanocomposite electrodes. (C)Specific capacitance verses current density of CoS@180°Cand RGO/CoS@180°C nanocomposite electrodes.

Conclusion

Overall, hydrothermal method was applied for the synthesis of CoS@180°Cand

RGO/CoS@180°Cnanocomposite. The XRD confirms the hexagonal crystal structure of CoS and RGO/CoS nanocomposites andare very well matched with JCPDS card No. 75-0605. The FTIR spectrum confirms the formation of CoS@180°Cand RGO/CoS@180°C nanocomposites through its characteristics peaks. The peak observed at 1092 cm^{-1}in FTIR and D, G band observed in Raman spectrum confirms the successful formation RGO in the RGO/CoS@180°C nanocomposites. The flower like shapes was seen through SEM and HRTEM images. The RGO/CoS@180°Cnanocomposites showed a higher specific capacitance value (650 F/g) than CoS@180°C electrode(467 F/g) for 10 mV/s indicated that the RGO/CoS@180°C nanocomposite is suitable material for supercapacitor appalications.

References

[1] Gkanas EI, Khzouz M. Numerical analysis of candidate materials for multi-stage metal hydride hydrogen compression processes. Renewable Energy. 2017 Oct , 1;111:484-93.

[2] Ho MY, Khiew PS, Isa D, Tan TK, Chiu WS, Chia CH. Charge storage performance of lithiated iron phosphate/activated carbon composite as symmetrical electrode for electrochemical capacitor. Current Applied Physics. 2014 Nov 1;14(11):1564-75.

[3] Sharma P, Bhatti TS. A review on electrochemical double-layer capacitors. Energy conversion and management. 2010 Dec 1;51(12):2901-12.

[4] Zuo W, Li R, Zhou C, Li Y, Xia J, Liu J. Battery-supercapacitor hybrid devices: recent progress and future prospects. Advanced science. 2017 Jul;4(7):1600539.

[5] Winter M, Brodd RJ. What are batteries, fuel cells, and supercapacitors. Chemical reviews. 2004 Oct 13;104(10):4245-70.

[6] Singu BS, Hong SE, Yoon KR. Ultra-thin and ultra-long α-MnO_2 nanowires for pseudocapacitor material. Journal of Solid State Electrochemistry. 2017Nov;21(11):3215-20.

[7] Khandare L, Terdale S. Gold nanoparticles decorated MnO_2 nanowires for high performance supercapacitor. Applied Surface Science. 2017 Oct 1;418:22-9.

[8] Tao F, Zhao YQ, Zhang GQ, Li HL. Electrochemical characterization on cobalt sulfide for electrochemical supercapacitors. Electrochemistry Communications. 2007 Jun 1;9(6):1282-7.

[9] Li Y, Liu S, Chen W, Li S, Shi L, Zhao Y. Facile synthesis of flower-like cobalt sulfide hierarchitectures with superior electrode performance for supercapacitors. Journal of Alloys and Compounds. 2017 Jul 25;712:139-46.

[10] Ranaweera CK, Wang Z, Alqurashi E, Kahol PK, Dvornic PR, Gupta BK, Ramasamy K, Mohite AD, Gupta G, Gupta RK. Highly stable hollow bifunctional cobalt sulfides for flexible supercapacitors and hydrogen evolution. Journal of Materials Chemistry A. 2016;4(23):9014-8.

[11] Zhang L, Wu HB, Lou XW. Unusual CoS 2 ellipsoids with anisotropic tube-like cavities and their application in supercapacitors. Chemical communications. 2012;48(55):6912-4.

[12] Xing JC, Zhu YL, Zhou QW, Zheng XD, Jiao QJ. Fabrication and shape evolution of CoS_2 octahedrons for application in supercapacitors. Electrochimica Acta. 2014 Aug 1;136:550-6.

[13] Lin JY, Tsai YT, Tai SY, Lin YT, Wan CC, Tung YL, Wu YS. Pulse-reversal

deposition of cobalt sulfide thin film as a counter electrode for dye-sensitized solar cells. Journal of The Electrochemical Society. 2012 Dec 4;160(2):D46.

[14] Raj CJ, Rajesh M, Manikandan R, Sim JY, Yu KH, Park SY, Song JH, Kim BC. Two-dimensional planar supercapacitor based on zinc oxide/manganese oxide core/shell nano-architecture. Electrochimica Acta. 2017 Sep 1;247:949-57.

[15] Zhang J, Chen Z, Wang Y, Li H. Morphology-controllable synthesis of 3D $CoNiO_2$ nano-networks as a high-performance positive electrode material for supercapacitors. Energy. 2016 Oct 15;113:943-8.

[16] Zhu J, Zhou W, Zhou Y, Cheng X, Yang J. Cobalt sulfide/reduced graphene oxide nanocomposite with enhanced performance for supercapacitors. Journal of Electronic Materials. 2019 Mar;48(3):1531-9.

[17] Wu W, Qi W, Zhao Y, Tang X, Qiu Y, Su D, Fan H, Wang G. Hollow CeO_2 spheres conformally coated with graphitic carbon for high-performance supercapacitor electrodes. Applied Surface Science. 2019 Jan 1;463:244-52.

[18] Zheng Y, Xu J, Zhang Y, Yang X, Zhang Y, Shang Y. Nitrogen-doped carbon nanotube supported double-shelled hollow composites for asymmetric supercapacitors. New Journal of Chemistry. 2018;42(1):150-60.

[19] Akbulut S, Yilmaz M, Raina S, Hsu SH, Kang WP. Advanced supercapacitor prototype using nanostructured double-sided MnO_2/CNT electrodes on flexible graphite foil. Journal of Applied Electrochemistry. 2017 Sep;47(9):1035-44.

[20] Qu B, Chen Y, Zhang M, Hu L, Lei D, Lu B, Li Q, Wang Y, Chen L, Wang T. β-Cobalt sulfide nanoparticles decorated graphene composite electrodes for high capacity and power supercapacitors. Nanoscale. 2012;4(24):7810-6.

[21] Shi J, Li X, He G, Zhang L, Li M. Electrodeposition of high-capacitance 3D CoS/graphene nanosheets on nickel foam for high-performance aqueous asymmetric supercapacitors. Journal of Materials Chemistry A. 2015;3(41):20619-26.

[22] Zhang Y, Liu J, Li Y, Yu M, Yin X, Li S. Enhancement of active anticorrosion via Ce-doped Zn-Al layered double hydroxides embedded in sol-gel coatings on aluminum alloy. Journal of Wuhan University of Technology-Mater. Sci. Ed.. 2017 Oct;32(5):1199-204.

[23] Zhu J, Zhou W, Zhou Y, Cheng X, Yang J. Cobalt sulfide/reduced graphene oxide nanocomposite with enhanced performance for supercapacitors. Journal of Electronic Materials. 2019 Mar;48(3):1531-9.

[24] Hummers Jr WS, Offeman RE. Preparation of graphitic oxide. Journal of the american chemical society. 1958 Mar;80(6):1339-.

[25] Wang Y, Li Y, Tang L, Lu J, Li J. Application of graphene-modified electrode for selective detection of dopamine. Electrochemistry communications. 2009 Apr 1;11(4):889-92.

[26] Zhou Q, Liu L, Guo G, Yan Z, Tan J, Huang Z, Chen X, Wang X. Sandwich-like cobalt sulfide–graphene composite–an anode material with excellent electrochemical performance for sodium ion batteries. RSC advances. 2015;5(88):71644-51.

[27] Yin PF, Sun LL, Gao YL, Wang SY. Preparation and characterization of Co_9S_8 nanocrystalline and nanorods. Bulletin of Materials Science. 2008 Aug;31(4):593-6.

[28] Krishnamoorthy K, Veerasubramani GK, Kim SJ. Hydrothermal synthesis, characterization and electrochemical properties of cobalt sulfide nanoparticles. Materials Science in Semiconductor Processing. 2015 Dec 1;40:781-6.

[29] Huang G, Chen T, Wang Z, Chang K, Chen W. Synthesis and electrochemical performances of cobalt sulfides/graphene nanocomposite as anode material of Li-ion battery. Journal of power sources. 2013 Aug 1;235:122-8.

[30] Tao F, Zhao YQ, Zhang GQ, Li HL. Electrochemical characterization on cobalt sulfide for electrochemical supercapacitors. Electrochemistry Communications. 2007 Jun 1;9(6):1282-7.

[31] Joshi JH, Kanchan DK, Joshi MJ, Jethva HO, Parikh KD. Dielectric relaxation, complex impedance and modulus spectroscopic studies of mix phase rod like cobalt sulfide nanoparticles. Materials Research Bulletin. 2017 Sep 1;93:63-73.

[32] Dar MA, Govindarajan D, Dar GN. Facile synthesis of SnS nanostructures with different morphologies for supercapacitor and dye-sensitized solar cell applications. Journal of Materials Science: Materials in Electronics. 2021 Aug;32(15):20394-409.

[33] Mala NA, Dar MA, Sivakumar S, Husain S, Batoo KM. Enhanced electrochemical properties of zinc and manganese co-doped NiO nanostructures for its high-performance supercapacitor applications. Inorganic Chemistry Communications. 2022 Aug 1;142:109661.

[34] Dar MA, Govindarajan D, Dar GN. Comparing the electrochemical performance of bare SnS and Cr-doped sns nanoparticles synthesized through solvothermal method. Physics of the Solid State. 2021 Sep;63(9):1343-50.

[35] Dar MA, Govindarajan D, Batoo KM, Siva C. Supercapacitor and magnetic properties of Fe doped SnS nanoparticles synthesized through solvothermal method. Journal of Energy Storage. 2022 Aug 25;52:105034.

[36] Dar MA, Mala NA, Dar GN, Kumar SS, Govindarajan D. Structural, optical, antibacterial analysis of Se Nanocomposite synthesized by precipitation method. Advances in Natural Sciences: Nanoscience and Nanotechnology. 2020 Sep 24;11(4):045001.

[37] Dar MA, Govindarajan D, Dar GN. Facile synthesis of SnS nanostructures with different morphologies for supercapacitor and dye-sensitized solar cell applications. Journal of Materials Science: Materials in Electronics. 2021 Aug;32(15):20394-409.

[38] Mala NA, Dar MA, Sivakumar S, Dar TA, Manikandan E. Review article on the performance of electrochemical capacitors when altered metals doped with nickel oxide nanomaterials. Journal of Nanoparticle Research. 2022 Nov;24(11):1-7.

[39] Fu Y, Wang X. Magnetically separable $ZnFe_2O_4$–graphene catalyst and its high photocatalytic performance under visible light irradiation. Industrial & Engineering Chemistry Research. 2011 Jun 15;50(12):7210-8.

eISSN1303-5150

[40] Muradov MB, Balayeva OO, Azizov AA, Maharramov AM, Qahramanli LR, Eyvazova GM, Aghamaliyev ZA. Synthesis and characterization of cobalt sulfide nanoparticles by sonochemical method. Infrared Physics & Technology. 2018 Mar 1;89:255-62.

[41] Ramachandran R, Felix S, Saranya M, Santhosh C, Velmurugan V, Ragupathy BP, Jeong SK, Grace AN. Synthesis of cobalt sulfide–graphene (CoS/G) nanocomposites for supercapacitor applications. IEEE transactions on nanotechnology. 2013 Aug 15;12(6):985-90.

[42] Mao J, Shu Q, Wen Y, Yuan H, Xiao D, Choi MM. Facile fabrication of porous CuS nanotubes using well-aligned [Cu (tu)] Cl· 1/2H2O nanowire precursors as self-sacrificial templates. Crystal Growth and Design. 2009 Jun 3;9(6):2546-8.

[43] Mao M, Mei L, Wu L, Li Q, Zhang M. Facile synthesis of cobalt sulfide/carbon nanotube shell/core composites for high performance supercapacitors. RSC Advances. 2014;4(23):12050-6.

[44] Peng S, Han X, Li L, Zhu Z, Cheng F, Srinivansan M, Adams S, Ramakrishna S. Unique cobalt sulfide/reduced graphene oxide composite as an anode for sodium-ion batteries with superior rate capability and long cycling stability. Small. 2016 Mar;12(10):1359-68.

[45] Zhang Y, Tian J, Li H, Wang L, Qin X, Asiri AM, Al-Youbi AO, Sun X. Biomolecule-assisted, environmentally friendly, one-pot synthesis of CuS/reduced graphene oxide nanocomposites with enhanced photocatalytic performance. Langmuir. 2012 Sep 4;28(35):12893-900.

[46] Suk JW, Kitt A, Magnuson CW, Hao Y, Ahmed S, An J, Swan AK, Goldberg BB, Ruoff RS. Transfer of CVD-grown monolayer graphene onto arbitrary substrates. ACS nano. 2011 Sep 27;5(9):6916-24.

[47] Wang YY, Ni ZH, Yu T, Shen ZX, Wang HM, Wu YH, Chen W, Shen Wee AT. Raman studies of monolayer graphene: the substrate effect. The Journal of Physical Chemistry C. 2008 Jul 24;112(29):10637-40.

[48] Yang Z, Zhang S, Zheng X, Fu Y, Zheng J. Controllable synthesis of copper sulfide for nonenzymatic hydrazine sensing. Sensors and Actuators B: Chemical. 2018 Feb 1;255:2643-51.

[49] Luo F, Li J, Yuan H, Xiao D. Rapid synthesis of three-dimensional flower-like cobalt sulfide hierarchitectures by microwave assisted heating method for high-performance supercapacitors. Electrochimica Acta. 2014 Mar 20;123:183-9.

[50] Ray RS, Sarma B, Jurovitzki AL, Misra M. Fabrication and characterization of titania nanotube/cobalt sulfide supercapacitor electrode in various electrolytes. Chemical Engineering Journal. 2015 Jan 15;260:671-83.

[51] Pandit B, Dubal DP, Sankapal BR. Large scale flexible solid state symmetric supercapacitor through inexpensive solution processed V_2O_5 complex surface architecture. Electrochimica Acta. 2017 Jul 10;242:382-9.

[52] Wang B, Park J, Wang C, Ahn H, Wang G. Mn_3O_4 nanoparticles embedded into graphene nanosheets: preparation, characterization, and electrochemical properties for supercapacitors. Electrochimica Acta. 2010 Sep 1;55(22):6812-7.

eISSN1303-5150